Garín, Moisés; Gamel, Mansur; Yli-Koski, Marko; Vähänissi, Ville; Rivera, Gerard; Savin, Hele; Martín, Isidro

Carrier mobility in crystalline germanium at high injection: experimental characterization of carrier-carrier scattering

Published in:
Solar Energy Materials and Solar Cells

DOI:
10.1016/j.solmat.2025.114011

Published: 15/01/2026

Document Version
Publisher's PDF, also known as Version of record

Solar Energy Materials & Solar Cells 295 (2026) 114011

Contents lists available at ScienceDirect

Solar Energy Materials and Solar Cells

journal homepage: www.elsevier.com/locate/solmat

Carrier mobility in crystalline germanium at high injection: experimental characterization of carrier-carrier scattering

Moisés Garín [a,*], Mansur Gamel [b], Marko Yli-Koski [c], Ville Vähänissi [c], Gerard Rivera [b], Hele Savin [c], Isidro Martín [b]

[a] Department of Engineering, Universitat de Vic—Universitat Central de Catalunya, Carrer de la Laura 13, 08500, Vic, Spain
[b] Universitat Politècnica de Catalunya, Carrer del Gran Capità, 08034, Barcelona, Spain
[c] Department of Electronics and Nanoengineering, Aalto University, Tietotie 3, 02150, Espoo, Finland

ARTICLE INFO

Handling Editor: Dr. Simon Philipps

ABSTRACT

The decay of the sum of electron and hole mobilities, $\mu_s = \mu_n + \mu_p$, due to carrier-carrier scattering was experimentally investigated in crystalline germanium (Ge) at high-injection conditions. Contactless measurements of the mobility sum as a function of the excess carrier density (Δn) in Ge were obtained using photoconductance decay methods. First, the measurement method was revised and improvements were introduced to ensure that $\mu_s(\Delta n)$ could be obtained for independent samples with improved accuracy. This method is successfully validated with crystalline silicon and, then, applied to Ge samples of different doping types and resistivity. The analysis of the data suggests that the mobility decay at high injection levels cannot be properly explained with the usual assumption of equal cross section for carrier-carrier and carrier-ion scattering events. Instead, we find the mobility sum due to carrier-carrier scattering to be inversely proportional to Δn according to the expression $8 \times 10^{20} \cdot \Delta n^{-1}$ cm^{2}V^{-1}s^{-1}. The limitations and potential error sources of the measurement method are discussed and, finally, the mobility model is used to improve lifetime analysis at high injection, allowing to estimate the ambipolar Auger recombination coefficient at $C_{amb} = 7 \times 10^{-31}$ cm^{6}s^{-1}.

1. Introduction

Carrier mobility is a fundamental physical property of materials defining carrier transport phenomena. Due to the evolution of technology, many solid-state devices are nowadays limited in speed and efficiency by the mobility of carriers. It is well understood that carrier mobilities are the combined effect of the different scattering mechanisms taking place in the material, most importantly, lattice scattering, ionized impurity scattering, and carrier-carrier (electron-hole) scattering. The carrier mobility in semiconductors was actively investigated in the middle of the 20th century, with many works reporting on carrier mobilities for both Silicon (Si) and Germanium (Ge) [1–7], most of them focusing on lattice and impurity scattering effects. At that time, it was also realized that electron-hole scattering should have a significant impact on the mobility of devices operating at high injection levels [8], roughly when the excess carrier density increases above 10^{16} cm^{-3}. At these high injection levels, the density of electrons and holes become similar and the sum of mobilities $\mu_s = \mu_n + \mu_p$ becomes the relevant physical parameter. To predict the impact of electron-hole scattering, in 1957 Fletcher proposed [9] to apply the classical theory of gasses, the mutual diffusion of two groups of oppositely charged particles, which led to a formulation very similar to the Conwell-Weisskopf approach [10] for the scattering by ionized impurities. Davies experimentally measured μ_s as a function of the injection level, Δn, in Ge by analyzing the potential difference after a pulse of current [11]. From these experiments, he deduced that the mobility term due to only electron-hole interactions follows the expression $\mu_s = 2.5 \times 10^{20} \cdot \Delta n^{-1}$ cm^{2}V^{-1}s^{-1}, which was also found to be consistent with the classical theory of gasses. A decade later, Dannhäuser and Krausse analyzed the decrease of the μ_s in Si at high injection levels [12,13], finding a good agreement with the experimental data using the formulation proposed by Fletcher.

Despite the significant research conducted on Ge in the 1950s, during the 1960s Si started to take over and, from there onward, the research community's interest focused primarily on Si for over half a century. However, Ge has recently regained interest due to both its high carrier mobility and low band gap, making it appropriate for high-speed

* Corresponding author.
E-mail address: moises.garin@uvic.cat (M. Garín).

https://doi.org/10.1016/j.solmat.2025.114011
Received 13 June 2025; Received in revised form 7 October 2025; Accepted 8 October 2025
Available online 17 October 2025

electronics and infrared photonic devices, respectively. A particular application that benefits from Ge characteristics is thermophotovoltaic (TPV) energy conversion [14,15]. In a TPV system, a high-temperature thermal emitter is placed in close vicinity to a low-band-gap photovoltaic cell, thus converting heat into electricity via thermally radiated photons. Since most of the energy in a TPV system is radiated in the infrared, the lower band gap of Ge makes it a more appropriate material for the application than Si. In addition, despite the relatively low temperature of the thermal radiation as compared to the sun's (around 1500K vs. 5700K, respectively), the large view factor present in TPV systems makes them operate at very high current densities, in the range of 1–10 A/cm^2, which is equivalent to that of high concentration solar photovoltaic systems. In this context, the high carrier mobilities in Ge, over three times larger than in Si, make it a very interesting material to handle the high current densities involved in TPV systems while ensuring a low parasitic series resistance and, thus, high efficiency.

Carrier mobilities can, in fact, impact the performance of TPV devices in subtle ways. Following the trends in standard photovoltaics, there is a growing interest in implementing Interdigitated Back-Contacted (IBC) TPV structures [16,17], as this maximizes output power while keeping all contacts in the back side, in direct contact with the cooling system. However, IBC structures can be limited by lateral transport in the semiconductor and, therefore, are particularly sensitive to the diffusion length and carrier mobilities. In addition, carrier mobilities are dependent on material quality and doping density and, most important to this work, at the high injection levels expected due to the large photon density, carrier mobilities can be noticeably reduced due to carrier-carrier scattering (CCS), impacting device performance. Furthermore, when characterizing TPV cells in the laboratory it is usually not feasible to replicate the real thermophotovoltaic operation conditions (high irradiance), with cell operations temperatures up to 80C, in practice omitting CCS effects and leading to an overestimation of carrier transport and system efficiency. In consequence, the precise characterization of carrier mobilities at high injection levels, including the CCS effects, is of paramount importance to accurately predict and optimize the efficiency of photovoltaic cells in real TPV conditions.

A more profound knowledge of CCS effects in Ge will also improve the accuracy in characterizing the excess carrier effective lifetime, τ_{eff}, as a function of excess carrier density, Δn. Considered as a "de facto" standard technique for Si, using the tools provided by Sinton Instruments, the quasi-steady-state photoconductance technique (QSSPC) [18] has been recently transferred to Ge [19] with great success. This technique determines both τ_{eff} and Δn by measuring the photoconductivity of the wafer through inductive coupling while illuminating the wafer with a flash lamp, providing τ_{eff} values in a wide Δn range typically spanning from 10^{14} cm^{-3} to 10^{17} cm^{-3}. In order to provide accurate results of both τ_{eff} and Δn, the QSSPC technique requires a precise knowledge of the semiconductor mobility, including the CCS effect.

Interestingly, it turns out that photoconductance measurements can also be used to determine the mobility of the material under test by comparing data obtained in QSSPC and Photoconductance Decay (PCD) conditions, both having a different dependence on carrier mobilities. Rougieux et al. presented this method for the first time using data obtained with a Sinton WCT100 and two different flash durations, the longer flash leading to QSSPC mode and the short one leading to PCD mode, and was able to determine $\mu_s(\Delta n)$ with some limitations [20]. By jointly analyzing with this technique a set of wafers of different resistivity, and assuming that the scattering cross section of two moving particles of different charge is the same as the cross section of a moving particle and an ionized impurity, Zheng et al. were able to characterize the μ_s in Si as a function of doping density, doping type, temperature, and injection level [21,22]. Recently, Krisztián et al. proposed combining data from three photoconductance decay techniques, namely transient, steady-state, and perturbation photoconductance, to directly determine $\mu_s(\Delta n)$ data claiming no model assumptions (model-free) [23].

In this work, we apply photoconductance decay methods to study the $\mu_s(\Delta n)$ in Ge, with a special focus on characterizing the mobility decay due to the CCS effect. In concrete, we have further refined the method by Rougieux so that $\mu_s(\Delta n)$ can be directly obtained with improved accuracy and from a single sample. After revisiting the theoretical background, we first validate the technique by applying it to Si substrates, where $\mu_s(\Delta n)$ is well known. Then, we apply the technique to Ge wafers of different types and doping densities ranging from intrinsic to moderately doped Ge. The analysis of the results concludes that, within the technique's limitations, the μ_s decay cannot be explained by the common assumption of equal scattering for carrier-carrier and mobile-ion interactions. On the other hand, a better consistency is found with mobility decay reported by Davies [11], *i.e.* inversely proportional to Δn. We discuss the possible limitations and potential improvements of the technique when applied to Ge wafers. Finally, we emphasize the significance of our CCS characterization by analyzing its impact on effective lifetime data at high injection and its implications for the accuracy of the estimation of the ambipolar Auger coefficient in Ge.

2. Theoretical background

2.1. Contactless determination of the mobility sum

The photoconductance decay method is a contactless technique that allows the characterization of the effective lifetime of photoexcited carriers through the analysis of the transient photoconductance under a short illumination pulse. In general, the effective lifetime is determined through the expression [24]

$$\tau_{eff}(\Delta n) = \frac{\Delta n(t)}{G(t) - \frac{d\Delta n(t)}{dt}}, \quad (1)$$

where τ_{eff} is the effective lifetime of photoexcited (excess) charge carriers, $G(t)$ is the average photogeneration rate, and $\Delta n(t)$ is the average excess carrier density in the bulk. This equation is valid for any light pulse duration, but there are two interesting limit cases. On the one hand, when the light pulse, typically from a flash lamp, has a time decay constant comparable to or larger than τ_{eff}, the method is known as Quasi-Steady-State Photoconductance decay (QSS) and there exists a balance between generation and recombination rates at all times. In this case, the derivative term in Equation (1) is considered negligible. On the other hand, when the flash time constant is much shorter than τ_{eff}, the method becomes a pure Photoconductance Decay technique (PCD), the idea here being to create an excess carrier density with a very short light pulse that quickly vanishes, leaving generated carriers to freely recombine. Now, the G(t) term disappears from Equation (1), and τ_{eff} becomes dependent exclusively on the decay of Δn. Notice that all variables involved in Equation (1) depend on time either directly or indirectly. For clarity, we will omit the time dependence from all variables and equations from now on. Clarifications on the variables' dependence will be added in the main text when required.

It should be stressed that Equation (1) deals with average quantities and, as a result, the obtained effective lifetimes will not depend on the flash decay time (either QSS or PCD extremes) as long as Δn can be assumed constant throughout the volume of the substrate under measurement. In other words, the results will be accurate when the diffusion length is comparable to or greater than the thickness of the wafer under test [25]. For Si and Ge substrates, this can be safely assumed for all practical wafer thicknesses and lifetime values thanks to the high carrier mobility, especially in the case of Ge [19]. For the sake of generality, in this work we will consider a PCD measurement to be one with a decay time noticeably shorter than the QSS counterpart but with a generation rate that might not always be negligible. This generalization will enable us to analyze data at high injection levels, where carrier-carrier scattering is strongest, but the PCD flash might still be present. Equation (1) can be rewritten for each case as:

$$\tau_{QSS}(\Delta n) = \frac{\Delta n}{G_{QSS} - \frac{d\Delta n_{QSS}}{dt}} \tag{2}$$

and

$$\tau_{PCD}(\Delta n) = \frac{\Delta n}{G_{PCD} - \frac{d\Delta n_{PCD}}{dt}}. \tag{3}$$

Notice that here Δn works as an independent variable for the lifetime in both cases, but its derivative with time differs as it depends on the flash time constant, hence the subscripts QSS and PCD in the derivatives. The generation rates are also distinguished by QSS and PCD subscripts.

The average photocarrier excess density, Δn, is not directly measured but determined from the photoconductance, $\Delta\sigma$, through

$$\Delta n = \frac{\Delta\sigma + \left(1 - \frac{\mu_s}{\mu_{s0}}\right)\sigma_0}{qw\mu_s}, \tag{4}$$

where $\Delta\sigma$ and σ_0 are, respectively, the photo- and dark conductance of the wafer, w is the wafer thickness, $\mu_s = \mu_n + \mu_p$ is the mobility sum at the given Δn, and μ_{s0} is the mobility sum in darkness ($\Delta n = 0$). It is crucial to notice that the σ_0 term in Equation (4) is usually disregarded, which assumes that the mobility is independent of Δn; however, this is generally not true, as demonstrated in this work. Under illumination, the conductance tends to increase due to the excess carrier density but, at the same time, there is a decrease in the mobilities due to CCS, which affects both thermal equilibrium carriers as well as the photogenerated ones, which needs to be taken into account. In consequence, the time derivative of Δn becomes

$$\frac{d\Delta n}{dt} = \frac{1}{qw\mu_s}\left(\frac{d\Delta\sigma}{dt} - \frac{(\Delta\sigma + \sigma_0)}{\mu_s}\frac{d\mu_s}{dt}\right). \tag{5}$$

Equating Equations (2) and (3), as the effective lifetime is unique ($\tau_{QSS}(\Delta n) = \tau_{PCD}(\Delta n)$), we obtain

$$G_{QSS} - \frac{d\Delta n_{QSS}}{dt} = G_{PCD} - \frac{d\Delta n_{PCD}}{dt}, \tag{6}$$

and taking into account Equations (4) and (5) we get to the general differential equation

$$\begin{aligned} &qw(G_{QSS} - G_{PCD})\mu_s^2 + \left(\frac{d\Delta\sigma_{PCD}}{dt} - \frac{d\Delta\sigma_{QSS}}{dt}\right)\mu_s \\ &- (\Delta\sigma + \sigma_0)\left(\frac{d\mu_{s,PCD}}{dt} - \frac{d\mu_{s,QSS}}{dt}\right) = 0. \end{aligned} \tag{7}$$

This equation can be easily solved for μ_s if the time derivative of the mobility can be neglected [20], leading to

$$\mu_s = \frac{1}{qw(G_{QSS} - G_{PCD})}\left(\frac{d\Delta\sigma_{QSS}}{dt} - \frac{d\Delta\sigma_{PCD}}{dt}\right). \tag{8}$$

However, this assumption is only valid under certain specific conditions. The derivative of the mobility can be conveniently rewritten as

$$\frac{d\mu_s}{dt} = \left.\frac{d\mu_s}{d\Delta\sigma}\right|_{\Delta\sigma(t)} \cdot \frac{d\Delta\sigma}{dt}, \tag{9}$$

where it becomes apparent that $d\mu/dt$ will approach zero only when $d\mu/d\Delta\sigma$ approaches zero. This is the case at low and moderate injection levels, where μ_s is independent of Δn, but not at high injection, where carrier-carrier scattering becomes significant, and μ_s decreases with increasing Δn. Substituting Equation (9) into Equation (7) we obtain our final differential equation:

$$\begin{aligned} &qw(G_{QSS} - G_{PCD})\mu_s^2 - \left(\frac{d\Delta\sigma_{QSS}}{dt} - \frac{d\Delta\sigma_{PCD}}{dt}\right)\mu_s \\ &+ \left(\frac{d\Delta\sigma_{QSS}}{dt} - \frac{d\Delta\sigma_{PCD}}{dt}\right)(\Delta\sigma + \sigma_0)\frac{d\mu_s}{d\Delta\sigma} = 0. \end{aligned} \tag{10}$$

Simultaneously solving the above equation for μ_s and $d\mu_s/d\Delta\sigma$ at each $\Delta\sigma$ is complex and highly sensitive to noise in the experimental photogeneration and conductance data. In this work, we use an iterative approach to numerically solve it. At every iteration, μ_s is first determined assuming an estimation of $d\mu_s/d\Delta\sigma$ determined in the previous iteration. Next, the $d\mu_s/d\Delta\sigma$ estimation is updated based on that μ_s result. These two steps are repeated until self-consistency between μ_s and $d\mu_s/d\Delta\sigma$ is achieved. In the first iteration, we just assume $d\mu_s/d\Delta\sigma = 0$ and, consequently, μ_s can be directly calculated by applying Equation (8). In any other iteration the mobility μ_s is determined by solving the quadratic Equation (10) leading to

$$\mu_s = \frac{1 - \sqrt{1 - 4A(\Delta\sigma + \sigma_0)\frac{d\mu_s}{d\Delta\sigma}}}{2A}, \tag{11}$$

where

$$A = qw(G_{QSS} - G_{PCD})\left(\frac{d\Delta\sigma_{QSS}}{dt} - \frac{d\Delta\sigma_{PCD}}{dt}\right)^{-1}. \tag{12}$$

To improve convergence and minimize the noise related issues, given that μ_s smoothly depends on $\Delta\sigma$, a smoothed $d\mu_s/d\Delta\sigma$ estimation is obtained by fitting the obtained $\mu_s(\Delta\sigma)$ with a selected mobility model at each iteration.

2.2. Optical factor modeling

The photoconductance decay techniques, both QSS and PCD with no negligible generation rate (Eq. (1)), require knowing both the wafer's conductance and the generation rate within its volume. While the conductance is directly measured through inductive coupling, the generation rate is indirectly determined by sensing the light intensity through a calibrated reference cell with

$$G = V_{ph}k_{S/V}\frac{J_{ref}}{qw}f_{opt}, \tag{13}$$

where G is the estimated generation rate, V_{ph} is the photovoltage signal provided by the reference cell, $k_{S/V}$ is a calibration constant that scales the photovoltage to equivalent suns of illumination intensity on the wafer, $J_{ref} = 38$ mAcm^{-2} is a reference short-circuit current for a standard Si cell under 1 sun, q is the elementary charge, w is the thickness of the wafer under test, and f_{opt} is the optical factor.

Any discrepancy between the absorption of the wafer under test, at one sun equivalent illumination, and the reference J_{ref} value is accounted for by the optical factor, which can be defined as

$$f_{opt} = \frac{q\int a\Phi_\lambda d\lambda}{J_{ref}}, \tag{14}$$

where λ is the wavelength of light, a is the absorptance of the wafer as a function of λ, and Φ_λ is the spectral photon flux of the flash lamp. It is important to notice that f_{opt} is subject to multiple effects that can be attributed to both the wafer under test and the equipment itself. On the one hand, it includes changes in the total absorption of the wafer due to, for instance, a particular surface texturing or anti-reflective coating and, most importantly, a change to a different bulk material. On the other hand, it also includes changes due to deviations between the flash lamp and the sun's reference spectra, as well as differences between the spectral absorption of the wafer and the reference cell. Furthermore, the optical factor will ultimately account for any uncertainty in the equipment calibration.

3. Experimental

In order to get reliable results of the carrier-carrier scattering in Ge, we have prepared a set of Ge wafers of different types and resistivity and with various surface treatments. In addition, we have also prepared a set

of Si wafers for verification purposes. Si wafers are used as a test material to verify the measurement procedure before analyzing the Ge results, as Si is a much better studied material and there is a broader literature on the mobility vs. injection level dependence. A wafer with black nanotexture, both for Si and Ge, was prepared for the purpose of calibrating the optical factor, as described in the results. Black wafers were not used in the mobility study. Table 1 summarizes the prepared sample set.

Samples were prepared at UPC or Aalto labs following standard procedures. A detailed description of the individual processes is beyond the scope of this work and is described elsewhere [26–29]; the following is a brief description of the general procedure with Ge wafers. Only new wafers were used straight from the box. Before processing, wafers undergo a standard cleaning based on hydrochloric acid solution to remove native oxides. For the samples with black Ge, the nanotexture is created on the front surface by a deep reactive ion etching (DRIE) step [30]. Regarding surface passivation, the SiO_2 and Al_2O_3 layers are grown simultaneously on both surfaces of the wafers by atomic-layer-deposition (ALD). In the case of SiC, the layers were grown on both surfaces by successive plasma-enhanced chemical vapor deposition (PECVD) processes. When required, samples went directly from PECVD to ALD equipment, or vice-versa, without any delay or additional processing.

The effective lifetime of the samples was measured using a Sinton WCT-120 equipment with the original flash lamp (Quantum QF-32 flash bulb) and the FPS-300 power supply. Measurements were taken with 400 Ws setting (HI flash mode). The flash bulb distance from the stage was 35 cm. Two measurements were taken for each sample with different flash lamp configurations: one with a long decay flash (1/1 mode; flash energy 400 Ws) and another with a short decay flash (1/64 mode: flash energy 400/64 Ws). The characteristic decay time of a long flash, used in QSS-PC measurements, is roughly 4 ms, while the short flash, used in PCD measurements, has a characteristic time of about 40 μs. It is worth noticing that we have samples with lifetimes similar to the characteristic time of both long and short flash durations. As a result, we cannot assume a pure QSS or PCD formulation in general. This is why our mathematical formalism relies on the most general case, using two measurements with different flash durations, without assuming either to be a pure PCD (zero generation). Finally, from the measurements we only use the raw conductivity and photogeneration data.

4. Results and discussion

4.1. Determination of the optical factor

The contactless determination of μ_s requires precise knowledge of the generation in order to provide reliable absolute μ_s values, which in turn requires an accurate characterization of the optical factor (f_{opt}) of each sample. In other words, the method is sensitive to both μ_s and f_{opt}. In fact, it is a common procedure for Si wafers to determine f_{opt} by matching a QSS and PCD measurement provided $\mu_s(N_D,N_A,\Delta n)$ is already well known [31,32]; in our case, this is obviously not directly applicable. However, since we are interested in the carrier-carrier scattering, present at medium and high Δn values, we can use the lowest injection data, around 10^{15} cm^{-3}, to estimate f_{opt} by using the electron and hole mobility models found in the literature as a function of doping. In particular, we considered the mobility parametrization used by Sinton Instruments [21] for Si and the parametrization by Berghuis [33] for Ge. It should be noted that that the data used here is the same as that used to determine the mobility. At excess carrier densities around 10^{15} cm^{-3}, carrier-carrier scattering cannot be fully neglected. To minimize errors, we include in this process an estimation of the CCS using the selected mobility model under test. By default, if nothing else is stated, CCS will be estimated by adding Δn to the doping density in the low-injection mobility model, in the case of Si, and by considering the CCS model proposed in this work, in the case of Ge.

Table 1 includes the f_{opt} values obtained with this method, where we processed the raw measurements considering the general Equation (4) for maximum accuracy, as it impacts the optical factors obtained. To validate the optical factor estimations, we have also determined f_{opt} through numerical calculations of the wafer absorption using the definition in Equation (14) and considering the flash spectrum shown in the supplementary information (see Figure S1). In the case of wafers with polished surfaces, absorption calculations were performed using a Transfer Matrix Method (TMM) formulation considering that the wafer is surrounded by air, *i.e.* assuming that the top surface of the measurement stage does not reflect any transmitted light back to the wafer. For the front-surface black-nanotextured wafers, previous experiments have demonstrated that such black nanotextures can be very efficient for (1) reducing reflection to nearly zero in a very broad wavelength range and (2) scattering light within the wafer, boosting absorption close to the $4n^2$ (perfect scattering) limit [34]. Performing precise numerical calculations of absorption for the nanotextured case is neither easy nor practical in this work. Therefore, as a compromise, we have considered the average between the two extreme cases: the ideal $4n^2$ absorption limit and the absorption obtained through TMM calculations assuming zero reflection at the front surface. Experimental and calculated f_{opt} values show a reasonably good linear correlation, as seen in Fig. 1, supporting the consistency of both methods. Moreover, for Si the calculated f_{opt} values nicely match the experimental ones, following a nearly perfect 45° correlation line. Notice, however, that the calculated f_{opt} values for Ge are about 18 % higher than the experimental ones. This is most probably due to the uncertainty in the spectrum of the flash lamp and would indicate that the spectrum used for calculations has about 18 % larger IR content than the real one. This, however, does not invalidate the methodology to estimate the optical factor and, in consequence, in the rest of the article we will use the experimental estimations of f_{opt}. It is worth emphasizing that this will ensure that the mobilities determined with our procedure asymptotically match the values from the literature low-injection model [33]. This, however, does not undermine the results

Table 1
List of wafers and corresponding treatments used in the experiment. DSP stands for double side polished surface finish. The terms bSi and bGe stand for black Si and black Ge nanotexture applied on the front surface, the back surface being polished. Passivation layers are symmetrical for all wafers. Effective lifetime, τ_{eff}, figures correspond to the minimum experimental values obtained at low injection ($\Delta n = 10^{15}$ cm^{-3}).

Wafer	Mat.	Type	Thick. (μm)	ρ (Ω·cm)	Surface	Surface passivation	τ_{eff} @ $\Delta n = 10^{15}cm^{-3}$	f_{opt}
Ge#1	Ge	N	189	21.5	DSP	Al_2O_3 (20 nm)	300 μs	0.74
Ge#2	Ge	N	295	29	DSP	SiO_2 + Al_2O_3 (20 nm + 20 nm)	2.3 ms	0.73
Ge#3	Ge	P	169	1.3	DSP	Al_2O_3 + SiC + Al_2O_3 (50 nm + 45 nm + 20 nm)	1 ms	1.07
Ge#4	Ge	P	175	1.3	DSP	SiO_2 + $Al2O_3$ (20 nm + 20 nm)	330 μs	0.79
Ge#5	Ge	P	175	0.13	DSP	i-aSiC + Al_2O_3 + SiC (2 nm + 50 nm + 45 nm)	510 μs	1.15
bGe	Ge	N	304.5	17.6–39.1	bGe	Al_2O_3 (20 nm)	11μs	1.28
Si#1	Si	N	350	3.5	DSP	SiO_2 (87 nm)	85 μs	0.80
Si#2	Si	N	350	3.5	DSP	SiO_2 (87 nm)	420 μs	0.76
Si#3	Si	N	280	2.5	DSP	Al_2O_3 (50 nm)	3.5 ms	0.76
Si#4	Si	P	285	2.6	DSP	Al_2O_3 (50 nm)	3.5 ms	0.72
bSi	Si	N	280	3	bSi	Al_2O_3 (20 nm)	>15 ms	1.04

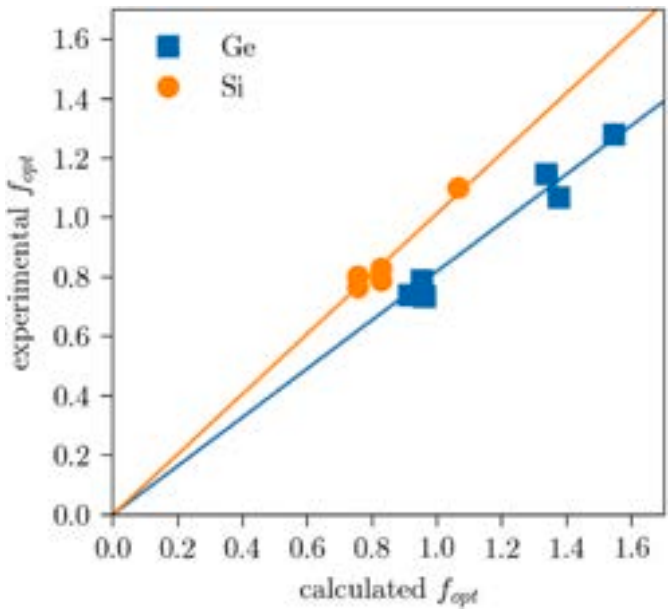

Fig. 1. Calculated vs. experimental values of the optical factor (f_{opt}) for the Si and Ge wafers used in the experiments. Symbols correspond to experimental data, while the solid lines correspond to linear regressions constrained to cross the origin.

at high injection. Moreover, an inaccurate mobility model assumption leads to an inconsistency between the selected model and the resulting experimental data, as we show in the next section.

4.2. Validation of the method

In order to validate the contactless determination of the mobility sum as a function of the injection level, we will first analyze and discuss the results for Si wafers, as there is a larger amount of data available in the literature. We applied the contactless determination of $\mu_n+\mu_p$ to every sample individually using the optical factor values determined at low injection as described earlier and considering the same mobility parametrization for Si as in the WCT-120 software [21]. The results are summarized in Fig. 2 in symbols. Lines represent the mobility sum as a function of Δn from the used parametrization. As the figure clearly shows, the experimental decay of $\mu_n+\mu_p$ clearly follows the model considered. Using other alternative Si mobility models from the literature [21,22,35–37] leads to similar results.

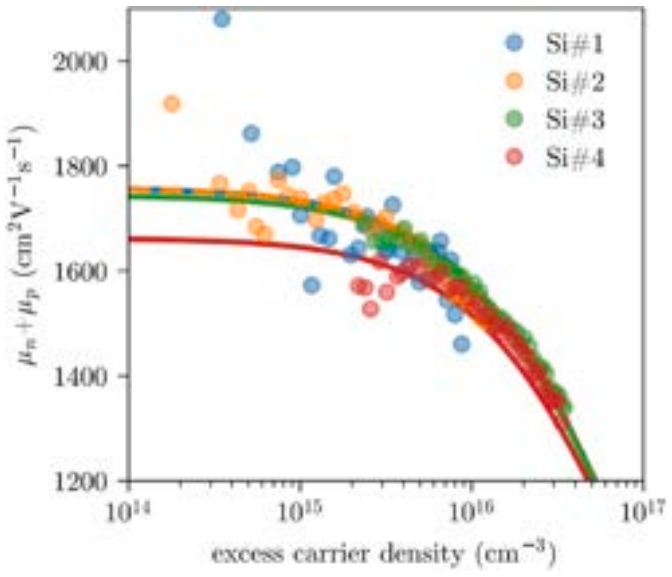

Fig. 2. Mobility sum ($\mu_n+\mu_p$) values for Si wafers. Symbols correspond to experimental values and lines correspond to theoretical values considering the mobility parametrization used by Sinton's WCT-120 software [21].

The data in Fig. 2 correspond to a single flash (PCD and QSS) using the standard IR pass filter provided by Sinton Instruments. ($\lambda_{cut\text{-}off} = 650$ nm) and no additional neutral filters. This allows for the determination of $\mu_n+\mu_p$ over approximately one Δn decade, with higher Δn values obtained for wafers with larger τ_{eff} and f_{opt} values. Notice that the noise in the mobility sum increases at decreasing Δn values as one would expect due to the reduced signal-to-noise ratio in the input data. In addition, the overall noise of the resulting data also depends on the lifetime of the sample, with noise increasing with decreasing wafer lifetime. This is because the denominator of Equation (11) becomes small when τ_{eff} is reduced. In the limit, with τ_{eff} approaching zero, both measurements would be in identical quasi-steady-state situation, breaking the assumptions of the method, and the denominator of Equation (11) becoming zero.

4.3. Ge results

After validating the measurement procedure with the Si wafers, we now apply it to the Ge samples described in Table 1. As a first step, we have taken the same assumption as in Si; this is, assuming that mobile-ion interactions have the same behavior as electron-hole interactions. In other words, using $N + \Delta n$ as an independent variable. The results are shown in Fig. 3 in symbols, where we have used the optical factors shown in Table 1, while solid lines correspond to the calculated mobility. As can be seen in Fig. 3, unlike the Si results, the experiments do not align well with this theoretical assumption. In the experiments, at the lower injection range $\mu_s(\Delta n)$ seems flatter than theoretically expected, while the decay seems shifted to slightly larger Δn values and with a steeper decay. Another even more noticeable anomaly is the fact that the very low doped N-type wafers (Ge#1 and Ge#2) present a CCS decay starting at lower Δn values than the rest of the wafers. In fact, for the very low doped wafers we would expect a greater mobility in darkness, but the current assumption for CCS scattering draws the mobility very close to that of the low doped ones. This could explain the

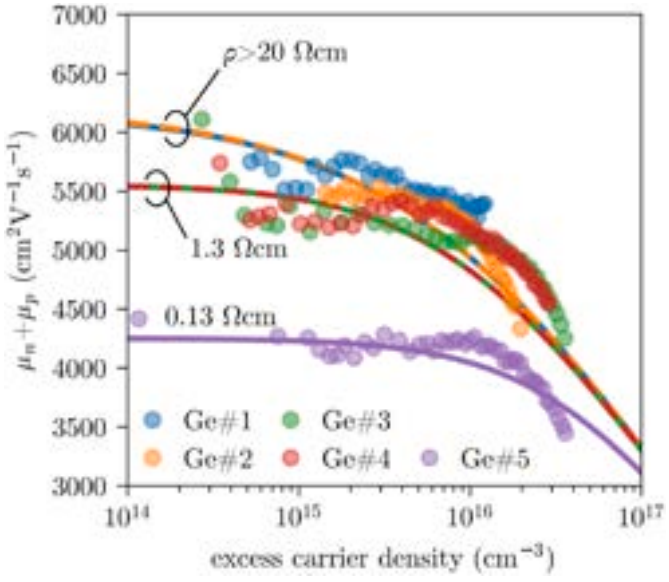

Fig. 3. Mobility sum ($\mu_n+\mu_p$) values for five Ge wafers. Symbols correspond to experimental values and lines correspond to calculations under the assumption of equal cross section for electron-hole and mobile-ion interactions and considering the low-injection mobility parametrization by Berghuis [33].

seemingly early CCS effect, as a wrong assumption in the $\mu_s(\Delta n)$ dependence couples to the results through the optical factor, pinning the measured mobility to the assumed model at the low injection range, as explained in section 4.1.

Driven by the above observations, we have switched to a formulation separating ion scattering and CCS scattering with

$$\mu_n = \left(\mu_{n0}^{-1} + \mu_{np}^{-1}\right)^{-1}, \tag{15}$$

$$\mu_p = \left(\mu_{p0}^{-1} + \mu_{np}^{-1}\right)^{-1}, \tag{16}$$

where μ_{n0} and μ_{p0} are the dark mobilities, in the absence of carrier-carrier scattering, which are functions of the doping using the Caughey & Thomas equation with Berghuis parametrization, and μ_{np} is the mobility due to carrier-carrier scattering, which can be determined with the expression

$$\mu_{np} = \frac{A\left(\frac{T}{300}\right)^{3/2}}{\sqrt{np}\cdot\log\left\{1 + B(pn)^{-1/3}\left(\frac{T}{300}\right)^{-2}\right\}}, \tag{17}$$

with A and B being constants. This last equation is very similar to the classical Conwell and Weisskopf formula [10], and can be derived applying the classical theory of gasses on the mutual diffusion of two groups of oppositely charged particles [9,38,39].

Despite only having two parameters, our data does not allow to determine both parameters due to the strong negative slope obtained at high injection. This leads to arbitrary large values of B, in effect making the logarithmic term independent of carrier density, leading to an inverse dependence on carrier density at high injection. Furthermore, an inverse dependence on carrier density was already observed in the past for Ge [11]. In consequence, assuming high injection ($n = p = \Delta n$), equation (17) can be reduced to:

$$\mu_{np} = \frac{D}{\Delta n}\left(\frac{T}{300}\right)^{3/2}, \tag{18}$$

where D is the unique empirical constant. This study is limited to room ($T = 300$ K) temperature and, therefore, the $(T/300)^{3/2}$ term will be omitted from now on. However, although out of the scope of this work, the expected $T^{3/2}$ temperature dependence may be useful to extrapolate the results to the typical operation temperature of TPV cells, that can operate at temperatures up to 80 °C, similar to standard PV cells. Finally, it is important highlighting that, at high injection level, the mobility sum will approach the expression $\mu_s = \mu_n + \mu_p \approx 2 \times D\Delta n^{-1}$.

We reprocessed the Ge data using the above mobility model with parameter D as an independent variable. For any particular D value, we first recompute the f_{opt} of the wafers and then recalculate the mobility sum, finally checking the consistency level (*i.e.* the degree of overlap) between the obtained values and the assumed model. The best results are shown in Fig. 4, which were obtained for a $D = 4 \times 10^{20}$ $cm^{-1}V^{-1}s^{-1}$. Larger D values shift the carrier-carrier effect to larger injection levels, beyond our experimental data, while lower D values both disrupt the correlation of the f_{opt} data and shift the CCS below experimental results. In terms of mobility sum, our result can be rewritten as $\mu_s = 8 \times 10^{20}\cdot\Delta n^{-1}$ $cm^2V^{-1}s^{-1}$. This result is close to the one provided by Davies [11] for the low-doped Ge region in a p^+-L-n^+ structure, which is the only work, to our knowledge, reporting experimental data for the mobility sum in Ge. In that work, he characterizes the mobility sum in the low-doped region by analyzing the differential potential across the device after a current pulse in the forward direction. In concrete, he reports that the mobility sum due to CCS can be expressed as a function of Δn as $\mu_s = 2.5 \times 10^{20}\cdot\Delta n^{-1}$ $cm^2V^{-1}s^{-1}$, with a mobility sum at low injection of $\mu_{n0}+\mu_{p0} = 4800$ $cm^2V^{-1}s^{-1}$. Despite the differences in material quality and measurement technique, this result is similar to the one reported hereby, same order of magnitude, and it reinforces the conclusions of this work. Our results, however, indicate a weaker carrier-carrier scattering effect, around three times, as compared to Davies' results.

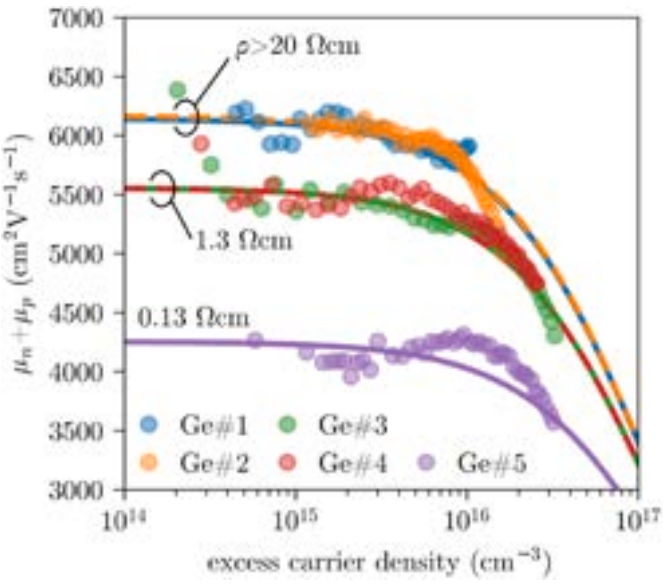

Fig. 4. Mobility sum (μ_n+μ_p) values for Ge wafers. Symbols correspond to experimental values and lines correspond to the proposed model with $D = 4 \times 10^{20}$ $cm^{-1}V^{-1}s^{-1}$.

In the results shown in Fig. 4, the very low-doped wafers now clearly exhibit the highest mobility values, with the CCS effect not kicking in until around 10^{16} cm^{-3}, making the mobility behavior more coherent in the whole sample set. However, there are still some differences between the model and experimental data that need to be mentioned. The most prominent is the effect of CCS at the highest injection levels, which seems to be stronger than expected according to the model. We think that this might be due to an artifact in the measurements at very high injection levels. In particular, during the initial moments of the flash, the condition of homogeneous excess carrier density is not met. In other words, during the very initial moments of the flash, carriers do not have time to distribute through the wafer, jeopardizing the full validity of the equations. To mitigate this we limit the data to the range were the signal of the reference cell and the photoconductance signal are both strictly decreasing, discarding the initial transient. However, we believe that this effect might still be present at the highest injection levels, and needs to be further investigated in the future. Additionally, we accept a certain generation level in the PCD measurement to reach very high-injection levels. Even though our formulation includes generation in the PCD, its large derivative term in the PCD measurement at the high-injection range might induce errors in the data processing. Furthermore, during the processing of the data, both the mobility and its derivative need to be deduced, which requires filtering the derivative through model fitting. This process is not perfect and can introduce artifacts when the fitting of the smoothing model is not optimal. In order to accurately analyze the CCS at the highest possible injection levels, careful analysis of these potential error sources needs to be performed, which is beyond this current work. Finally, our method imposes the mobility at low injection through the particular dark mobility model considered during the derivation of the optical factor. As a result, any inconsistency between these models will also bias and distort the results.

To emphasize the practical significance of the CCS effect, we now demonstrate its impact on effective lifetime data at high injection. Firstly, it is important to note that the mobility model influences both PCD and QSS measurements, with a more pronounced effect in the latter

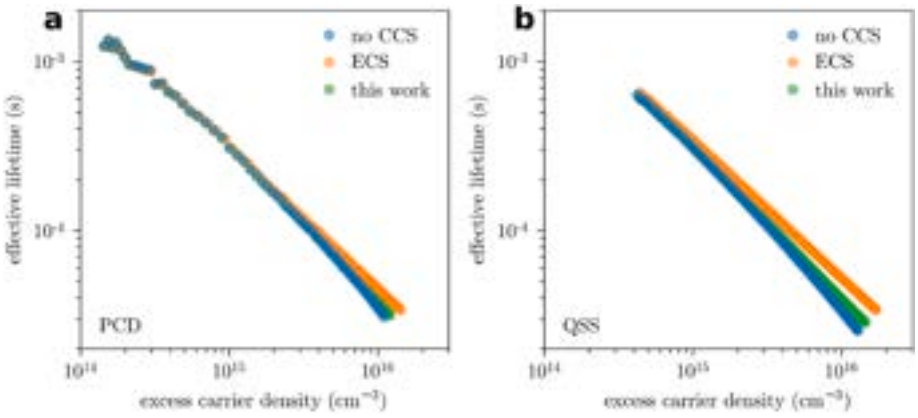

Fig. 5. Experimental effective lifetime of sample Ge#1 obtained with a short flash (**a**) and a long flash (**b**). Three different mobility models were considered: (blue) no carrier-to-carrier scattering, (orange) equal cross-section (ECS) for mobile carriers and fixed ions, and (green) the mobility model deduced in this work. (For interpretation of the references to colour in this figure legend, the reader is referred to the Web version of this article.)

case (see Fig. 5 as an example with a low doped Ge wafer, Ge#1). The impact of the CCS model is particularly noticeable at high injection levels in QSS measurements, as mobility strongly affects both τ_{eff} and Δn values. At Δn values above 10^{16} cm^{-3}, the differences in τ_{eff} between models can result in errors close to 100 % in the worst-case scenario. For PCD measurements, however, the effect appears smaller. While the mobility model affects Δn estimation in the same way as in QSS data, it subtly influences τ_{eff} through $\mathrm{d}\mu/\mathrm{d}\Delta n$, altering τ_{eff} in a way that coincidentally follows the natural τ_{eff} decay, thereby reducing the total error within the measured range.

A precise characterization of the $\tau_{\text{eff}}(\Delta n)$ curve at high injection levels also enables a better quantification of the Auger recombination. Auger recombination is an intrinsic process that dominates bulk recombination in indirect gap semiconductors under both high-injection conditions and in moderately to highly doped substrates. Despite its significance, quantifying Auger recombination is challenging, as it cannot be directly measured and must be separated from the rest of recombination processes. Black and Macdonald proposed estimating the ambipolar Auger coefficient, C_{amb}, from $\tau_{\text{eff}}(\Delta n)$ data in high-quality crystalline silicon wafers passivated with dielectric layers that induce strong accumulation or inversion [41]. Under these assumptions, the total recombination rate expression can be rearranged as

$$\left(\tau_{\text{eff}}^{-1}-\tau_{\text{SRH}}^{-1}\right)(p_0+n_0+\Delta n)^{-1}=C_{\text{amb}}\Delta n+C_p p_0+C_n n_0+(1-f_r)B_{\text{rad}}+\frac{2}{w}\frac{J_{0s}}{qn_i^2}, \tag{19}$$

where τ_{SRH} is the bulk lifetime due to Shockley-Read-Hall recombination, p_0 and n_0 are the thermal equilibrium concentration of holes and electrons, ni is the intrinsic concentration, C_{p} and C_{n} are the Auger coefficient for the electron-hole-hole and electron-electron-hole interactions, $C_{\text{amb}} = C_{\text{p}} + C_{\text{n}}$, Brad is the radiative coefficient, f_{r} is the fraction of radiatively emitted photons reabsorbed, and $J_{0\text{s}}$ is the surface saturation current density. Given that in the right-hand term only the first term depends on Δn, C_{amb} can be estimated from the slope of a plot representing $\left(\tau_{\text{eff}}^{-1}-\tau_{\text{SRH}}^{-1}\right)(p_0+n_0+\Delta n)^{-1}$ vs. Δn. Notice that either τ_{SRH} needs to be high enough to be negligible, or it needs to be estimated through self-consistency or by other means.

To further emphasize the relevance of precise CCS characterization in Ge, we applied Black & Macdonald's method to estimate C_{amb} using our data. However, the higher radiative recombination in Ge, combined with the fact that current surface passivation technology in Ge is not as efficient as in Si, makes the application of this method very challenging. This is because Auger recombination becomes less relevant across most of the injection range. From our heterogeneous sample set, the wafer with the highest lifetime at high injection is sample Ge#5. As shown in the fitting in Fig. 6b, at $\Delta n > 10^{16}$ cm^{-3}, surface, radiative and Auger recombination processes become comparable, with Auger becoming dominant for $\Delta n > 4 \times 10^{16}$ cm^{-3}. In this unfavorable situation, using QSS data, which has a better signal-to-noise ratio, becomes more convenient. Fig. 6a shows the $\left(\tau_{\text{eff}}^{-1}-\tau_{\text{SRH}}^{-1}\right)(p_0+n_0+\Delta n)^{-1}$ vs. Δn curves considering (blue) no CCS, (orange) equal cross-section for ions and free carriers (ECS), and (green) the CCS parametrization in this work. In Fig. 6a the curve was offset to pass through the origin, correcting for surface and radiative recombination, and τ_{SRH} was obtained through self-consistency fitting of the curve, as shown in Fig. 6b. As seen in the results, despite the relatively low lifetime of the sample compared to the Auger lifetime, data considering the CCS data from this work achieve better results when applying Black & Macdonald's method, with an excellent fit in both panels. With our CCS data we obtained $C_{\text{amb}} = 7 \times 10^{-31}$ cm^{6}s^{-1} (1.9×10^{-30} cm^{6}s^{-1} with no CCS and 8.5×10^{-31} cm^{6}s^{-1} for ECS assumption), which is within the range of reported values in the literature [41–49], with C_{amb} between 4×10^{-30} cm^{6}s^{-1} and 10^{-31} cm^{6}s^{-1}. In fact, our results seem to indicate that Auger recombination would be overestimated when CCS effects on mobility are not accurately considered. In any case, accurate quantification of Auger recombination is beyond the scope of this work, which would require a new wafer set specially prepared for this purpose and accurate accounting of additional effects such as Coulomb enhancement at high injection.

5. Summary

In this work, we have experimentally studied the decay of the mobility in Ge due to carrier-carrier scattering at high injection levels. The mobility has been measured as a function of the excess carrier density using a contactless photoconductance decay technique. For this purpose, the method proposed by Rougieux has been revised and improved so that it can be applied reliably at high injection levels. For higher accuracy, the optical factor of the samples was theoretically calculated and calibrated using wafers with different optical absorption. The measurement method was successfully verified by applying it to Si wafers, obtaining an excellent agreement between measurements and literature data. The analysis of the data for Ge wafers suggests that the mobility sum due to CCS can be modeled by the expression $8 \times 10^{20} \cdot \Delta n^{-1}$ cm^{2}V^{-1}s^{-1}. Furthermore, the results suggest that the typical assumption of equal cross section for electron-hole and mobile-ion scattering interactions is inadequate in Ge. Finally, the proposed mobility model at high injection has been shown to provide a more

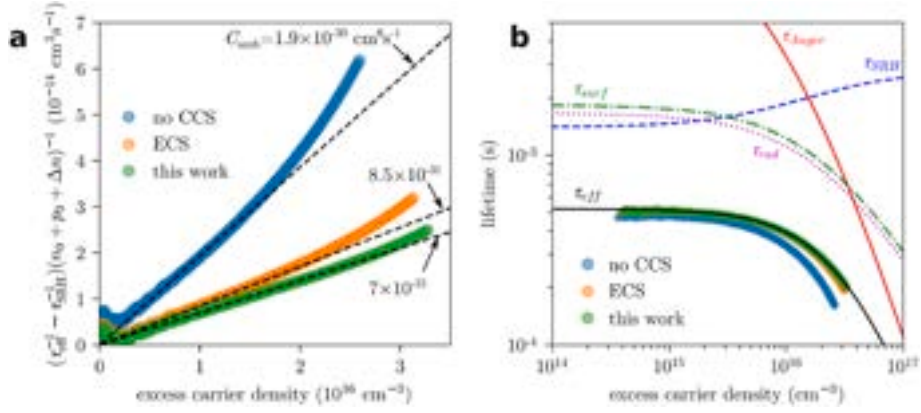

Fig. 6. (**a**) Representation of experimental $(\tau_{\text{eff}}^{-1}-\tau_{\text{SRH}}^{-1})(p_0+n_0+\Delta n)^{-1}$ vs. excess carrier density (Δn) after correcting for surface and radiative recombination components with an offset. Dashed lines correspond to a linear fit to the data in the low Δn range. (**b**) Fitting of the τ_{eff} model to the experimental data obtained using the mobility model from this work and the ambipolar Auger coefficient deduced for the data using the mobility model from this work.

accurate lifetime data at high injection, which enabled to estimate the ambipolar Auger coefficient at $C_{\text{amb}} = 7 \times 10^{-31}$ cm^{6}s^{-1}.

CRediT authorship contribution statement

Moisés Garín: Writing – review & editing, Writing – original draft, Visualization, Validation, Supervision, Software, Project administration, Methodology, Investigation, Funding acquisition, Formal analysis, Data curation, Conceptualization. **Mansur Gamel:** Writing – review & editing, Investigation. **Marko Yli-Koski:** Writing – review & editing, Visualization, Methodology, Investigation, Conceptualization. **Ville Vähänissi:** Writing – review & editing, Validation, Methodology, Formal analysis. **Gerard Rivera:** Writing – review & editing, Investigation. **Hele Savin:** Writing – review & editing, Validation, Resources, Methodology, Conceptualization. **Isidro Martín:** Writing – review & editing, Validation, Supervision, Resources, Project administration, Methodology, Conceptualization.

Declaration of competing interest

The authors declare that they have no known competing financial interests or personal relationships that could have appeared to influence the work reported in this paper.

Acknowledgments

This work is part of the projects PID2020-115719RB-C21 (GETPV), PID2023-150209OB-C22 (TOMATE) and TED2021-131778B (TROPIC)) funded by MCIN/AEI/10.13039/5011000110033. Project TED2021-131778B (TROPIC) is also funded by European Union "NextGenerationEU"/PRTR. M. Y.-K., V. V. and H. S. acknowledge the financial support of the Research Council of Finland (#331313, #338974). The authors acknowledge the provision of facilities and technical support by Micronova Nanofabrication Centre in Espoo, Finland within the OtaNano research infrastructure at Aalto University.

Appendix A. Supplementary data

Supplementary data to this article can be found online at https://doi.org/10.1016/j.solmat.2025.114011.

Data availability

Data will be made available on request.

References

[1] H. Brooks, Scattering by ionized impurities in semiconductors, Phys. Rev. 83 (1951) 879.
[2] M.B. Prince, Drift mobilities in semiconductors. I. Germanium, Phys. Rev. 92 (1953) 681–687.
[3] M.B. Prince, Drift mobilities in semiconductors. II. Silicon, Phys. Rev. 93 (1954) 1204–1206.
[4] P.P. Debye, E.M. Conwell, Electrical properties of N-Type germanium, Phys. Rev. 93 (1954) 693–706.
[5] F.J. Morin, J.P. Maita, Conductivity and hall effect in the intrinsic range of germanium, Phys. Rev. 94 (1954) 1525–1529.
[6] H. Brooks, Theory of the electrical properties of germanium and silicon, Adv. Electron. Electron. Phys. 7 (1955) 85–182, https://doi.org/10.1016/S0065-2539(08)60957-9.
[7] D.M. Caughey, R.E. Thomas, Carrier mobilities in silicon empirically related to doping and field, Proc. IEEE 55 (1967) 2192–2193.
[8] R.N. Hall, Power rectifiers and transistors, Proceedings of the IRE 40 (1952) 1512–1518.
[9] N.H. Fletcher, The high Current limit for semiconductor junction devices, Proceedings of the IRE 45 (1957) 862–872, https://doi.org/10.1109/JRPROC.1957.278485.
[10] E. Conwell, V.F. Weisskopf, Theory of impurity scattering in semiconductors, Phys. Rev. 77 (1950) 388–390.
[11] L.W. Davies, Electron-hole scattering at high injection levels in germanium, Nature 194 (1962) 762–763.
[12] J. Krausse, Die abhängigkeit der trägerbeweglichkeit in silizium von der konzentration der freien ladungsträger – II, Solid State Electron. 15 (1972) 1377–1381.
[13] F. Danhäuser, Die abhängigkeit der trägerbeweglichkeit in silizium von der konzentration der freien ladungsträger – i, Solid State Electron. 15 (1972) 1371–1375.
[14] J. van der Heide, N.E. Posthuma, G. Flamand, W. Greens, J. Poortmans, Cost-efficient thermophotovoltaic cells based on germanium substrates, Sol. Energy Mater. Sol. Cell. 93 (2009) 1810–1816.
[15] M. Gamel, H.J. Lee, W. Rashid, P.J. Ker, L.K. Yau, M.A. Hannan, Md Z. Jamaludin, A review on thermophotovoltaic cell and its applications in energy conversion: issues and recommendations, Materials 14 (2021) 4944.
[16] M. Gamel, G. Rivera, G. López, M. Garín, I. Martín, Interdigitated Back Contacted c-Ge thermophotovoltaic devices, in: 15th TPV Conf., PS1.3, 2024. Madrid, Spain.
[17] A. Datas, Bifacial thermophotovoltaics energy conversion, ACS Photonics 10 (2023) 683–690.
[18] R.A. Sinton, A. Cuevas, Contactless determination of current-voltage characteristics and minority-carrier lifetimes in semiconductors from quasi-steady-state photoconductance data, Appl. Phys. Lett. 69 (1996) 2510.
[19] I. Martín, A. Alcañiz, A. Jiménez, G. López, C. del Cañizo, A. Datas, Application of quasi-steady-state photoconductance technique to lifetime measurements on crystalline germanium substrates, IEEE J. Photovoltaics 10 (2020) 1068–1075.
[20] F.E. Rougieux, P. Zheng, M. Thiboust, J. Tan, N.E. Grant, D.H. Macdonald, A. Cuevas, A contactless method for determining the carrier mobility sum in silicon wafer, IEEE J. Photovoltaics 2 (2012) 41–46.
[21] P. Zheng, F.E. Rougieux, D. Macdonald, A. Cuevas, Measurement and parameterization of carrier mobility sum in silicon as a function of doping, temperature and injection level, IEEE J. Photovoltaics 4 (2014) 560–565.
[22] P. Zheng, F.E. Rougieux, D. Macdonald, A. Cuevas, Parameterization of carrier mobility sum in silicon as a function of doping, temperature and injection level: extension to p-type silicon. 2014 IEEE 40th Photovoltaic Specialist Conference (PVSC), 2014, pp. 129–134. Denver, CO, USA.

[23] D. Krisztián, F. Korsós, G. Havasi, Simultaneously measurement of charge carrier concentration, mobility, and lifetime, Sol. Energy Mater. Sol. Cell. 260 (2023) 112461.
[24] H. Nagel, C. Berge, A.G. Aberle, Generalized analysis of quasi-steady-state and quasi-transient measurements of carrier lifetimes in semiconductors, J. Appl. Phys. 86 (1999) 6218.
[25] J. Brody, A. Rohatgi, A. Ristow, Review and comparison of equations relating bulk lifetime and surface recombination velocity to effective lifetime measured under flash lamp illumination, Sol. Energy Mater. Sol. Cells 77 (2003) 293–301.
[26] I. Martín, G. López, M. Garín, C. Voz, P. Ortega, J. Puigdollers, Effect of the thickness of amorphous silicon carbide interlayer on the passivation of c-Ge surface by aluminium oxide films, Surf. Interfaces 31 (2022) 102070.
[27] J. Isometsä, T.H. Fung, T.P. Pasanen, H. Liu, M. Yli-koski, V. Vähänissi, H. Savin, Achievingsurface recombination velocity below 10 cm/s in n -type germanium using ALD Al_2O_3, APL Mater. 9 (2021) 111113.
[28] H. Liu, T.P. Pasanen, O. Leiviskä, J. Isometsä, T.H. Fung, M. Yli-Koski, M. Miettinen, P. Laukkanen, V. Vähänissi, H. Savin, Plasma-enhanced atomic layer deposited SiO2 enables positive thin film charge and surface recombination velocity of 1.3 cm/s on germanium, Appl. Phys. Lett. 122 (2023) 191602.
[29] T.H. Fung, J. Isometsä, J.-P. Lehtiö, T.P. Pasanen, H. Liu, O. Leiviskä, P. Laukkanen, H. Savin, V. Vähänissi, Efficient surface passivation of germanium nanostructures with 1% reflectance, Nanotechnology 34 (2023) 355201.
[30] Toni P. Pasanen, J. Isometsä, M. Garin, K. Chen, V. Vähänissi, H. Savin, Nanostructured Germanium with >99% absorption at 300-1600 nm Wavelengths, Adv. Opt. Mater. 8 (2020) 2000047.
[31] T. Trupke, R.A. Bardos, Self-consistent determination of the generation rate from photoconductance measurements, Appl. Phys. Lett. 85 (2004) 3611.
[32] D. Macdonald, A. Cuevas, K. McIntosh, L. Barbosa, D. De Ceuster, Impact of Cr, Fe, Ni, Ti AND W Surface Contamination on Diffused and Oxidised N-type Crystalline Silicon Wafers" Proc. 20th, EU PVSEC, Barcelona, 2005, p. 627.
[33] W.J.H. Berghuis, Nanolayers for Germanium Surface Passivation Prepared by Atomic Layer Deposition and Chemical Vapor Deposition, Eindhoven University of Technology, 2022 [Phd Thesis 1 (Research TU/e/Graduation TU/e), Applied Physics and Science Education].
[34] M. Garín, T.P. Pasanen, G. López, V. Vähänissi, K. Chen, I. Martín, H. Savin, Black ultra-thin crystalline silicon wafers reach the $4n^2$ absorption limit – application to IBC solar cells, Small 19 (2023) 2302250.
[35] D.A. Clugston, P.A. Basore, PC1D version 5: 32-bit solar cell simulation on personal computers. 26th IEEE Photovoltaic Specialists Conf, Sept., 1997.
[36] W.R. Thurber, R.L. Mattis, Y.M. Liu, Resistivity-Dopant density relationship for boron-doped silicon, J. Electrochem. Soc.: Solid-State Science and Technology 127 (1980) 2291–2294.
[37] W.R. Thurber, R.L. Mattis, Y.M. Liu, The Relationship Between Resistivity and Dopant Density for Phosphorus- and Boron-Doped Silicon, SP 400–64, U.S. Department of Commerce/National Bureau of Standards, NBS, 1981.
[38] S.C. Choo, Theory of a forward-biased diffused-junction P-L-N Rectifier—-Part I: exact numerical solutions, IEEE Trans. Electron. Dev. ED-19 (1972) 954–965.
[39] J.M. Dorkel, Ph Leturq, Carrier mobilities in silicon semi-empirically related to temperature, doping and injection level, Sol. State Electron. 24 (1981) 821–825.
[41] L.E. Black, D.H. Macdonald, On the quantification of Auger recombination in crystalline silicon, Sol. Energy Mater. Sol. Cell. 234 (2022) 111428.
[42] R. Conradt, J. Aengenheister, Minority carrier lifetime in highly doped Ge, Solid State Commun. 10 (1972) 321–323.
[43] L. Huldt, Auger recombination in germanium, phys. stat. sol. (a) 24 (1974) 221.
[44] L. Huldt, Phonon-Assisted auger recombination in germanium, phys. stat. sol. (a) 33 (1976) 607.
[45] D. Poelman, P. Clauws, B. Depuydt, Chemical surface passivation of low resistivity p-type Ge wafers for solar cell applications, Sol. Energy Mater. Sol. Cells 76 (2003) 167–173.
[46] E. Gaubas, J. Vanhellemont, Dependence of carrier lifetime in germanium on resisitivity and carrier injection level, Appl. Phys. Lett. 89 (2006) 142106.
[47] E. Gaubas, M. Bauža, A. Uleckas, J. Vanhellemont, Carrier lifetime studies in Ge using microwave and infrared light techniques, Mater. Sci. Semicond. Process. 9 (2006) 781–787.
[48] A. Vossier, B. Hirsch, J.M. Gordon, Is Auger recombination the ultimate performance limiter in concentrator solar cells? Appl. Phys. Lett. 97 (2010) 193509.
[49] A. Uleckas, E. Gaubas, T. Ceponis, K. Zilinskas, R. Grigonis, V. Sirutkaitis, J. Vanhellemont, Analysis of Auger Recombination Characteristics in High Resistivity Si and Ge, Solid State Phenom. 178–179 (2011) 427–432.